PTHrP-derived Peptides Restore Bone Mass and Strength in Diabetic Mice: Additive Effect of Mechanical Loading

Marta Maycas[1,2], Kevin A McAndrews[1,3], Amy Y Sato[1], Gretel G Pellegrini[1], Drew M Brown, Matthew R Allen[1], Lilian I Plotkin[1,3], Arancha R Gortazar[4], Pedro Esbrit[2],* Teresita Bellido[1,3,5]*

[1]Department of Anatomy and Cell Biology, Indiana University School of Medicine, Indianapolis, Indiana.

[2]Instituto de Investigación Sanitaria-Fundación Jiménez Díaz, Madrid, Spain.

[3]Roudebush Veterans Administration Medical Center, Indianapolis, Indiana.

[4]Instituto de Medicina Molecular Aplicada-Universidad San Pablo CEU, Madrid, Spain.

[5]Department of Medicine, Division of Endocrinology, Indiana University School of Medicine, Indianapolis, Indiana.

To whom correspondence should be addressed.Teresita Bellido, PhD, 635 Barnhill Drive, Medical Science Building – Room 5045A, Indianapolis, IN 46022, Voice 317-274-7410, Fax 317-278-2040, tbellido@iupui.edu; Pedro Esbrit, PhD, Avda. Reyes Católicos, 2, 28040 Madrid, Spain, Voice 91 544 37 20 / 91 550 48 97, PEsbrit@fjd.es

The authors have declared that no conflict of interest exists.

This research was supported by the National Institutes of Health (R01-AR059357 to T.B.); the Veterans Administration (1 I01 BX002104-01 to T.B.); the Spanish Instituto de Salud Carlos III (PI11/00449 and RD12/0043/0008); and Universidad San Pablo CEU (emerging group). M.M. received short-term fellowships from The European Molecular and Biology Organization (EMBO), Conchita Rábago Foundation, and Boehringer Ingelheim; and was also supported by Spanish Ministerio de Economía y Competitividad (FI12/00458).

Abstract

There is an unmet need to understand the mechanisms underlying skeletal deterioration in diabetes mellitus (DM) and to develop therapeutic approaches to treat bone fragility in diabetic patients. We demonstrate herein that mice with type 1 DM induced by streptozotocin exhibited low bone mass, inferior mechanical and material properties, increased bone resorption, decreased bone formation, increased apoptosis of osteocytes, and increased expression of the osteocyte-derived bone formation inhibitor Sost/sclerostin. Further, short treatment of diabetic mice with parathyroid hormone related protein (PTHrP)-derived peptides corrected these changes to levels undistinguishable from non-diabetic mice. In addition, diabetic mice exhibited reduced bone formation in response to mechanical stimulation, which was corrected by treatment with the PTHrP peptides; and higher prevalence of apoptotic osteocytes, which was reduced by loading or by the PTHrP peptides alone, and reversed by a combination of loading and PTHrP peptide treatment. In vitro experiments demonstrated that the PTHrP peptides or mechanical stimulation by fluid flow activated the survival kinases ERKs and induced nuclear translocation of the canonical Wnt signaling mediator β-catenin; and prevented the increase in osteocytic cell apoptosis induced by high glucose. Thus, PTHrP-derived peptides crosstalk with mechanical signaling pathways to reverse skeletal deterioration induced by DM in mice. These findings suggest a crucial role of osteocytes in the harmful effects of diabetes on bone and raise the possibility of targeting these cells as a novel approach to treat skeletal deterioration in diabetes. Moreover, our study suggest the potential therapeutic efficacy of combined pharmacological and mechanical stimuli to promote bone accrual and maintenance in diabetic subjects.

KEY WORDS: diabetes, osteocytes, Sost/sclerostin, PTHrP, osteocyte apoptosis

Introduction

Diabetes mellitus (DM) is a highly prevalent disease with negative impact on the skeleton, which markedly increases fracture risk [1]. In subjects with type 1 DM (T1D), bone mass is consistently decreased, whereas in those with type 2 DM bone mass is usually normal or even high; but in both cases there are concomitant alterations in bone structure and strength that compromise bone quality [2]. Diabetic subjects show decreased bone formation and increased resorption due to complex and yet ill-defined mechanisms, including hyperglycemia and accumulation of advanced glycation end products, deficiency in insulin/insulin-like growth factor 1 secretion, and alterations in the parathyroid hormone (PTH)/Vitamin D axis. The morbidity and mortality associated with bone fractures are especially aggravated by alterations in fracture healing [3].

Earlier work demonstrated downregulation of PTH-related protein (PTHrP) and osteopenia in streptozotozin (STZ)-induced T1D in mice [4]. PTHrP is a ubiquitous cytokine with important functions in bone development and metabolism. Administration of PTHrP-derived peptides that interact with the same receptor than PTH and PTHrP (PTH1R), or the PTH-unrelated peptide PTHrP(107-139), exert osteogenic effects in osteopenic mouse models [5].

Mechanical stimulation, such as in physical exercise, is anabolic for the skeleton, while immobilization leads to bone loss. Accumulated evidence demonstrates that osteocytes are major cells responsible for bone adaptation to changes in mechanical force [6]. Osteocytes are located into lacunae within the mineralized matrix, and connect among themselves and osteoblasts and osteoclasts on the bone surface through a network of dendritic processes, allowing osteocytes to act as orchestrators of bone remodeling [7]. Mice with heterozygous Ins2Akita mutation, a spontaneous T1D model, show a reduction in osteocyte processes, increased spacing of lacunae, and deficient

bone formation in response to loading [8,9]. The same investigators reported that MLO-Y4 osteocytic cells exposed to high glucose showed impaired responses to mechanical stimulation *in vitro*. Further, we found increased osteocyte apoptosis in bone of STZ-induced diabetic CD1 mice, effect that was counteracted by treatment with N- and C-terminal PTHrP peptides for 2 weeks [10].

A central role of the PTH1R expressed in osteocytes is supported by studies in transgenic mice expressing an activated PTH1R in these cells, which exhibit high bone remodeling and increased bone mass, recapitulating the actions of PTH on the skeleton[11]. In contrast, mice lacking the PTH1R in mature osteoblasts/osteocytes show a deficient response to systemic PTH elevation [12]; and mice lacking the PTH1R in osteocytes exhibit impaired response to mechanical stimulation [13]. Further, PTHrP/PTH1R signaling is involved in fluid flow-induced survival of osteocytic cells in vitro [14].

In the present study, we demonstrate that short treatment with two different PTHrP-derived peptides restored in part the loss of bone mass and strength by targeting both bone formation and bone resorption, and worked additively with mechanical loading to enhance periosteal bone formation and to promote osteocyte survival in diabetic mice in vivo. Further, the PTHrP peptides together with mechanical stimulation, activate survival signaling and prevent the pro-apoptotic effect of high glucose in osteocytic cells in vitro. These findings suggest the potential therapeutic efficacy of combined pharmacological and mechanical stimuli to promote bone accrual and maintenance in diabetic subjects.

Materials and Methods

Animal model

One hundred and thirty three 3-month old male C57BL/6 mice (Harlan, Indianapolis, IN) randomized by spinal BMD were used in the study (**Figure 1A**). Mice were grouped housed (5 mice/cage) and fed a standard rodent diet (Harlan/Teklad #7001), received water ad-libitum and exposed to a 12h light/dark cycle. T1D was induced by 5 daily injections of STZ (45mg/kg i.p. in 50 mM citrate buffer, pH 4.5) or buffer alone (controls), followed by glucose measurements after 18 days to confirm T1D (nonfasting blood glucose >250 mg/dL) [(4)]. After 28 days to allow bone loss, diabetic mice were assigned to 3 groups, which received 3 daily s.c. injections of vehicle (50 mM KCl, pH 4.5), or 50 μg/kg PTHrP(1-37) or 7 μg/kg PTHrP(107-111) (Bachem, Bubendorf, Switzerland). Fifteen min after each injection, right ulna were loaded for 1 min, at 120 cycles/day at forces required to generate low, medium or high mechanical strains (see below). Mice were euthanized 15 days after the first loading bout; and bones were analyzed. Loading strains were determined in a previous experiment as previously published [(15-17)]. Ten 3-month-old male C57BL/6 mice (Harlan, Barcelona, Spain) received 5 daily injections of buffer (controls) or STZ (T1D) and sacrified after 4 weeks. Right forearms were dissected to expose the ulnar diaphysis, and a miniature single element strain gauge (EA-015DJ-120; Vishay, Inc.) was bonded to the midshaft. Forearms were placed in a computer-controlled electromagnetic mechanical actuator (Bose, Eden Prairie, MN), and exposed to cyclic axial compression using a 2-Hz haversine waveform. The peak force was progressively increased with each cycle, and ranged from 1.2 to 2.4 N. During loading, conditioned voltage output from the strain gauge and output from the load cell were recorded; and voltage output converted to strain using previously described calibration procedures.

From these data the force:strain relation was derived for both groups, and low, medium, and high loads for in vivo mechanical loading were calculated so that 1,995; 2,250 and 2,500 μstrain were generated for both genotypes. No significant difference in the strain/load ratio was found between control and T1D mice (947.7±118.6 and 864.3±92.2 με/N, respectively). Protocols were approved by the Institutional Animal Care and Use Committee at Fundación Jiménez Díaz, Spain according to the European Union guidelines, and the Institutional Animal Care and Use Committee of Indiana University School of Medicine, USA.

Bone turnover markers

Osteocalcin (OCN) (Alpha Aesar-Johnson Matthey Co. Ward Hill, MA) and C-telopeptide fragments of type I collagen (CTX) (RatLaps, Immunodiagnostic Systems Inc., Fountain Hills, AZ) were measured following manufacturer's instructions [18,19].

Bone mineral density (BMD) and microcomputerized tomography (μCT) analysis

BMD was measured by dual energy X-ray absorptiometry using a PIXImus II densitometer (GE Medical Systems, Lunar Division, Madison, WI) and μCT analysis at 6 μm-resolution was performed using a Scanco μCT 35 instrument (Scanco Medical, Brüttisellen, Switzerland) [18].

Biomechanical testing

Femoral 3-point bending was performed using a miniature bending apparatus [20]. Mechanical properties were determined from the load deformation curves using standard definitions. Cross-sectional moment of inertia and anterior-posterior diameter determined by μCT were used to calculate material level properties using standard equations.

Bone histology

Mice were injected with calcein and alizarin red (30 and 50 mg/kg; Sigma), 7 and 2 days before sacrifice, respectively [18]. Bones were dissected, fixed in 10% buffered formalin, and embedded in methyl methacrylate. Thick, 100-µm cross-sections at the ulnae mid-diaphysis ground to 40 µm; and thin, 5 µm longitudinal sections from L1-L3 vertebrae, were prepared for dynamic and static histomorphometric analysis, respectively. Analysis was performed using OsteoMeasure (OsteoMetrics Inc., Decatur, GA). The terminology and units used are those recommended by the Histomorphometry Nomenclature Committee of the American Society for Bone and Mineral Research [21]. Osteocyte apoptosis by TdT-mediated dUTP nick-end labeling (TUNEL; EMD Millipore, Billerica, MA) and sclerostin immunohistochemistry were performed on demineralized, paraffin embedded, consecutive 5 µm longitudinal sections of ulnae mid-diaphysis [19,22]. Immunohistochemistry was performed using anti-mouse sclerostin antibody (R&D Systems, Minneapolis, MN), or non-immune IgG as negative control, followed by rabbit anti-goat horseradish peroxidase-coupled antibody (Santa Cruz Biotechnology, Santa Cruz, CA). Color was developed with a diaminobenzidine substrate chromogen system (Dako Corp., Carpinteria, CA). In both cases, sections were counterstained with 2% methyl green, and observed under an Olympus BX51TRF microscope (Olympus America Inc., Center Valley, PA) at 400× magnification. The percentage of sclerostin-positive osteocytes was quantified in the medial region of the ulnae and analyzed using OsteoMeasure. Adipocyte area was quantified using the OsteoMeasure system (OsteoMetrics Inc., Decatur, GA) on the same ulnae sections stained for sclerostin and conterstained with 2% methyl green. Adipocytes within the marrow cavity were identified by morphology, and adipocyte area was corrected by bone marrow area.

RNA extraction and quantitative PCR (qPCR)

Total RNA was extracted from mouse tibiae using TRIzol (Invitrogen, Grand Island, NY), and cDNA was synthesized using the Invitrogen Superscript First-strand Synthesis System for RT-PCR. Gene expression was quantified by qPCR performed as described[18], using sets of primers and probes designed using the Assay Design Center (Roche Applied Science, Indianapolis, IN) or commercially available carried out in an ABI PRISM 7500 system (Applied Biosystems, Foster City, CA). Results were calculated for each sample using the cycle threshold (Ct) value, and were normalized against ribosomal protein S2 (ChoB) as housekeeping gene.

Cell culture

Osteocytic MLO-Y4 cells were grown at 20,000 cells/cm^2 on collagen-coated culture plates, as previously published [23,24]. Twenty four hours later, fresh culture medium was added with or without 25 mM high D-glucose (or L-glucose as osmotic control) and cells were cultured for another 24h-period, adding PTHrP peptides at 100 nM for the last 30 min. Subsequently, cells were subjected to mechanical stimulation by fluid flow with a shear stress of 10 dynes/cm^2 in an 8 Hz pulsatile manner for 10 min in a Flexcell® Streamer® shear stress device (Flexcell International Corp., Hillsborough, NC) [14,25].

MLO-Y4 cells were transfected with a mixture of two (si)RNA duplexes (each at 20 nM) against different target sequences in mouse PTH1R (siPTH1R) (Life Technologies, Carlsbad, CA, USA) using Lipofectamine RNAiMax (Life Technologies) overnight at 37°C. A si scramble (control siRNA-A; Santa Cruz Biotechnology) was used as a negative control. The VEGFR2 antagonist SU5416 (1 mM; Sigma– Aldrich, St. Louis, MO) was added 30 min before PTHrP (107-111) addition.

In vitro apoptosis assessment

After fluid flow, MLO-Y4 were exposed to the pro-apoptotic agent etoposide (50 μM) and/or the PTHrP peptides, in the absence of serum for 6 h and subsequently fixed with neutral buffer formalin. Apoptosis was assessed by enumerating cells expressing nuclear green fluorescent protein (nGFP) exhibiting chromatin condensation and nuclear fragmentation under a fluorescence microscope [24]. Cell death was quantified by Trypan blue uptake of nonadherent cells pooled with adherent cells. The percentage of apoptotic cells in the absence of etoposide was 3.6±1.3 %.

Western blot analysis

For Bcl-2 western analysis, total protein lysates from MLO-Y4 where obtained using RIPA buffer, pH 8.0 (Sigma-Aldrich), supplemented with protease inhibitor cocktail P8340 (Sigma–Aldrich) and phosphatase inhibitor cocktail Set II (Calbiochem, La Jolla, CA). For β-catenin and ERK western analysis, nuclear protein extracts were obtained using the subcellular protein fractionation kit (Pierce, Rockford, IL), according to manufacturer's instructions. Proteins (25-30 μg) were separated by PAGE as previoiusly published [25]. Blots were probed with rabbit polyclonal anti-Bcl-2 (1:1000, Santa Cruz Biotechnology), anti-β-catenin (Abcam, Cambridge, MA), anti-ERK1/2 (Cell Signaling, Beverly, MA), or anti-lamin B1 (Abcam) antibodies. Mouse monoclonal anti-α-tubulin (Sigma Aldrich) or rabbit polyclonal anti-lamin B1 (Abcam) antibodies were used as loading control. Subsequently, membranes were incubated with the corresponding horseradish peroxidase-coupled anti-rabbit antibodies (Santa Cruz Biotechnology); and developed with ECL system (GE-Amersham Pittsburgh, PA). Band intensities were quantified by densitometry.

Statistical analysis

Seven-10 mice/condition were used to achieve enough statistical power for the detection of >2% changes in bone mass and strength induced by the treatments, based on previous studies [16,18,26]. Means ± standard deviations (SD) are reported; $p<0.05$ were considered significant. Statistical analysis was performed using GraphPad Prism (GraphPad Software, La Jolla, CA) and SigmaStat (SPSS Science, Chicago, IL). Data were analyzed by one- or two-way ANOVA and, if a significant effect or interaction was found, it was further examined by performing pair-wise multiple comparisons with Tukey tests. For the loading experiments, differences between loaded and non-loaded ulnae were evaluated by paired t-test. For *in vitro* experiments, data represent 2-3 experiments carried out in triplicate and analyzed by Kruskal-Wallis test followed by Mann-Whitney test.

Results

The skeletal deterioration exhibited by T1D mice is corrected by treatment with PTHrP(1-36) or PTHrP(107-111) peptides.

The experimental design of the *in vivo* study is shown in **Figure 1A.** All mice were diabetic after 3 weeks following STZ injections, as shown by increased glucose concentration in the serum **(Figure 1B)**. Mice remained hyperglycemic until the end of the study. The average body weight at the beginning of the study was 26.9 g, ranging from 21.7 to 30.3 g; whereas at the end of the study, diabetic mice exhibited decreased body weight. Treatment with either PTHrP peptide did not alter glycemia or body weight**.**

Diabetic mice showed decreased total, spinal, and femoral BMD (t1) by 6-9% **(Figure 1C** and **D)**. A further decrease compared to control non-diabetic mice in spinal and femoral BMD of 4.1 and 3.8%, respectively, was observed 15 days later (t2-t1) in vehicle-treated diabetic mice compared to control mice, but not in diabetic mice treated with either PTHrP peptide **(Figure 1E)**. μCT analysis revealed that cortical bone area (BA/TA) and cortical thickness (Ct.Th) were decreased (by 16%) and marrow cavity area was increased (by 11%) in the femur mid-diaphysis in diabetic mice; and that all parameters were normalized by treatment with the PTHrP peptides **(Figure 1F)**. Further, diabetic mice showed a decrease of 50% in cancellous bone (BV/TV) and of 27% in trabecular thickness (Tb. Th) in the distal femur compared to controls (**Figure 1G**). PTHrP(107-111) partially restored BV/TV and both peptides increased trabecular thickness compared to untreated diabetic mice.

The decrease in cancellous bone is accompanied by a decrease of 33-39% in osteoblast number (NOb/BS), osteoblast surface (ObS/BS), and osteoid surface (OS/BS), and by an increase of 32-63% in osteoclast number (NOc/BS, 49%),

osteoclast surface (OcS/BS, 32%), and eroded surface (ES/BS, 63%) in diabetic mice **(Figure 2A).** These changes were reversed by treatment with the PTHrP peptides. On the other hand, osteocyte density (NOt/BV) was not affected by any of the treatments. Consistent with the changes in osteoblast number, mineralizing surface (MS/BS) and mineral apposition rate (MAR) were decreased in vertebral cancellous bone of diabetic mice, resulting in a reduction in bone formation rate (BFR/BS) of 49% **(Figure 2B).** Both PTHrP peptides reversed these changes to levels undistinguishable from control non-diabetic mice. Bone formation indexes were not significantly reduced on the endocortical surface of the ulna in diabetic mice. Nevertheless, both PTHrP peptides increased by 61-54% endocortical bone formation compared to control non-diabetic mice **(Figure 2C)**.

Biomechanical parameters of femoral cortical bone were next evaluated by the three point bending test. Diabetic mice exhibited a significant reduction in mean energy to failure (51%), ultimate force (43%) and stiffness (32%), compared to control mice **(Figure 3A).** Furthermore, the material properties of bone ultimate stress, toughness, and Young's modulus were also decreased in diabetic mice by 23-43% **(Figure 3B).** Treatment with either PTHrP normalized the altered bone mechanical properties in the diabetic mice **(Figure 3).**

The alterations in bone resorption and formation and in gene expression in bone exhibited by T1D mice are corrected by PTHrP peptides.

Evaluation of circulating bone remodeling markers at the end of the study showed increased CTX (50%) and decreased osteocalcin (62%) in the diabetic mice; and these changes were at least partially reversed by PTHrP treatment **(Figure 4A)**. Bones from T1D mice exhibited ~80% decreased expression of osterix, which is

expressed in a fraction of osteoblast precursors and also highly expressed in osteoblasts and osteocytes, and the PTHrP peptides completely reversed this decrease (**Figure 4B**). The expression of the Wnt/β-catenin antagonists Sost and Dkk1 was markedly increased in T1D mice by 575 and 380 %; and whereas the peptides did not alter Dkk1 expression, they significantly decreased Sost expression to levels similar to those of control mice. The expression of the cytokine OPG was decreased by ~80 %, and no significant changes in RANKL expression were detected, compared to controls, resulting in a 53% increase in the RANKL/OPG ratio **(Figure 4C)**. Treatment with PTHrP peptides increased OPG and reduced the RANKL/OPG ratio to levels no significantly different from control mice. TRAP gene expression was increased by 155% in T1D mice and the peptides decreased it to values no significantly different than control mice. Similar pattern of expression compared to OPG was founds for connexin 43 (Cx43), another gene regulated by Wnt singnaling (**Figure 4C**). In contrast, the expression of Axin2, BMP4 and cyclin D1, other Wnt target genes, was not affected by any treatment (not shown). The levels of PTHrP and PTH1R in vertebra and tibia were not altered in diabetic mice treated with vehicle or with the PTHrP peptides (**Figure 4D**).

The increased marrow adiposity exhibited by T1D mice is reversed by PTHrP peptides.

T1D mice also exhibited an increase of approximatedly 600% in the area covered by adipocytes in the bone marrow compared to control mice (**Figure 5**); and treatment with the PTHrP peptides reversed adipocyte area corrected per marrow area. Similar findings were observed when adipocyte number was quantified (not shown).

Moreover, none of the mechanical loading regimens altered marrow adiposity in controls or T1D mice treated with vehicle or the PTHrP peptides (not shown).

PTHrP peptides act additively with mechanical loading to increase bone formation in diabetic mice and to prevent osteocyte apoptosis *in vivo* and *in vitro*.

We next evaluated the ability of mechanical stimulation to induce an osteogenic response in control and diabetic mice, in combination with treatment of PTHrP peptides (**Figure 6**). Mechanical stimulation at medium and high magnitude increased periosteal bone formation in control mice by 166 and 457%, respectively, whereas diabetic mice only showed a response to the highest magnitude of strain of 248%. Treatment with the each PTHrP peptide increased bone formation in diabetic mice to similar levels than mechanical stimulation alone at high magnitude. Moreover, the increase in bone formation induced by each PTHrP peptide was higher in ulnae subjected to the high magnitude of loading compared to non-loaded ulnae (765-1019% versus 425-515%, respectively), demonstrating an additive effect of the treatment and mechanical stimulation in T1D mice **(Figure 6C)**.

Sclerostin protein expression in osteocytes of diabetic mice was similar to that of control mice; and it was not altered by treatment with the PTHrP peptides (**Figure 7A**). On the other hand, the % of sclerostin positive osteocytes was reduced by mechanical stimulation at medium and high intensities in control mice (by 25 and 49 %, respectively), consistent with earlier findings [16,27] (**Figure 7A** and **B**). In contrast and consistent with the less sensitivity to loading demonstrated on bone formation, the highest magnitude of mechanical strain was required to reduce (by 29%) sclerostin expression in diabetic mice, with or without treatment with the PTHrP peptides.

Osteocyte apoptosis in diabetic mice was about 30% compared to 20% in control mice **(Figure 7C)**. Loading at medium and high magnitude of strain reduced significantly osteocyte apoptosis in control mice to about 15% and at the high magnitude also reduced apoptosis in diabetic mice from 33% to 25%. Further, peptide treatment reduced the elevated prevalence of osteocyte apoptosis of diabetic mice to levels indistinguishable from controls. Moreover, the peptides in combination with high magnitude mechanical strain further decreased osteocyte apoptosis to values observed in loaded ulna of nondiabetic controls.

Consistent with the increased osteocyte apoptosis found in T1D hyperglycemic mice, MLO-Y4 osteocytic cells cultured in high levels of glucose potentiated the effect of the pro-apoptotic agent etoposide **(Figure 8A)**. Addition of the PTHrP peptides decreased apoptosis induced by etoposide as well as the further increase in apoptosis induced by high glucose. In addition, mechanical stimulation provided by fluid flow decreased etoposide-induced apoptosis and culture in high glucose containing medium hampered the protective effect of mechanical stimulation. Moreover, the pro-apoptotic effect of high glucose was counteracted by each PTHrP peptide. We showed earlier that the anti-apoptotic effect of PTHrP (1-37) depends on the expression of the PTHR1 [(14)]. On the other hand, the anti-apoptotic effect of PTHrP (107-111) was not altered by silencing PTH1R but instead was abolished by inhibition of the VEGF receptor with SU5416 (**Figure 8B**). Mechanical stimulation increased the expression of the anti-apoptotic protein Bcl-2 under normal glucose levels, but not with high glucose (**Figure 8C**). Moreover, PTHrP (1-37), but not PTHrP (107-111), increased Bcl-2 in the presence of high glucose, under both static conditions and in cultures subjected to fluid flow, adding further support to a different mechanism of action of the two PTHrP peptides. These findings are consistent with earlier evidence demonstrating that

promotion of cell survival by PTHrP or PTH through the PTH1R in chondrocytes or osteoblasts, respectively, is mediated by increased Bcl-2 [28,29]. Although high glucose did not affect the expression of Bcl-2 in cultures maintained under static conditions, it decreased Bcl-2 in cultures subjected to fluid flow. In the presence of high glucose, PTHrP (107-111) or fluid flow alone did not increase Bcl-2 levels, but combination of the two stimuli did.

Exposure of osteocytic cells to high glucose prevented the increase induced by mechanical stimulation in nuclear accumulation of β-catenin or ERKs, two events associated with the pro-survival action of several stimuli in osteocytes [14,25,30,31] (**Figure 8D**). However, high glucose did not affect the basal levels of the proteins. In addition, the PTHrP peptides induced nuclear accumulation of β-catenin and ERKs in cells cultured under normal or high glucose levels.

Discussion

We characterized herein, at the tissue, cellular and molecular levels, the mechanisms underlying the bone fragility associated with diabetes and the counteracting beneficial effects of two peptides derived from PTHrP, alone or in combination with mechanical stimulation, using a mouse model of T1D. Our findings demonstrate that diabetes increases bone resorption, decreases bone formation and induces apoptosis of osteocytes, resulting in decreased bone mass and deterioration of the microarchitecture and the mechanical properties of bone. The PTHrP-derived peptides were effective in attenuating the deleterious effects of diabetes; and they exhibited additive effects in conjunction with mechanical stimulation. Our findings show that diabetes *in vivo* and high glucose *in vitro* increased apoptosis of osteocytes; and that the PTHrP peptides or mechanical loading attenuate this effect. Moreover, the PTHrP peptides promote osteocyte viability by activating similar mechanisms than those induced by mechanical stimulation, which involve stabilization of β-catenin, the mediator of the canonical Wnt signaling, as well as activation of the ERK survival kinases. However, PTHrP (1-37) acts through the PTH1R whereas PTHrP (107-111) does not and requires activation of the VEGFR2 receptor. Diabetic mice also exhibited high levels of expression of mRNA transcripts for Sost/sclerostin, an antagonist of canonical Wnt signaling expressed in osteocytes that potently inhibits bone formation. Taken together, these findings strongly suggest a crucial role of osteocytes in the harmful effects of diabetes on bone and raise the possibility of targeting osteocytes as a novel approach to treat skeletal deterioration in diabetes.

A higher magnitude of strain was needed to induce periosteal bone accrual and to inhibit osteocyte apoptosis after loading in diabetic mice compared to control non-diabetic mice, demonstrating that diabetic bone is less responsive to mechanical forces.

Remarkably, co-treatment with the PTHrP peptides was able to increase the anabolic and anti-apoptotic effect on osteocytes induced by loading *in vivo*. Likewise, the PTHrP peptides prevented the impaired response to fluid flow exhibited by osteocytic cells cultured in high glucose levels on viability and pro-survival signaling. Moreover, high glucose differentially influences the response to fluid flow versus the PTHrP peptides, supporting the notion that different mechanisms are activated by the two stimuli upstream of Bcl-2, β-catenin, and ERKs. Taking together, these findings suggest a crosstalk between mechanical stimuli and PTHrP-activated signaling that additively counteracts the damaging actions of diabetes on osteoblast activity and osteocyte survival.

Decreased osteoblast number and function has consistently been reported in the STZ-induced diabetic animal models as well as in other insulin-dependent diabetic models [4,10,32-36] On the other hand, the role of osteoclasts in this setting is less clear. Similar to our findings, bone resorption is increased in short-term diabetes in rats or severe diabetes in some, but not all, mouse strains [37,38]. However, several studies in T1-diabetic rodents show decreased osteoclast activity [37]. Moreover, exposure of murine pre-osteoclasts to high glucose has been shown to inhibit both osteoclastogenesis and osteoclast activity *in vitro* [39]. Thus, differences in disease severity, mouse strain, species and even age might contribute to the different bone resorption status observed in various studies using diabetic models [40,41].

Recent studies point to alterations in the Wnt/β-catenin pathway as an important mechanism underlying T1D-related bone dysfunction [10,36,42]. Two inhibitors of the pathway, namely Dkk1 and Sost, were shown to be overexpressed in the long bones of diabetic mice. Furthermore, transcripts for both inhibitors were also up-regulated in bones from STZ-induced diabetic rats, together with inhibition of Wnt signaling and

osteoblastogenesis, associated with insulin deficiency [36]. We also found that Sost mRNA was increased in bones of diabetic mice. Although we could not detect significant changes in the percentage of osteocytes expressing sclerostin in the current study, we cannot exclude the possibility that the expression of the protein per osteocyte is decreased in diabetic mice. Nevertheless, higher magnitude of load is necessary to reduced sclerostin levels in diabetic mice compared to control non-diabetic mice, indicating that the mechanisms involved in regulating sclerostin expression are affected by diabetes. Moreover, treatment with the PTHrP peptides reversed the up-regulation of Sost mRNA expression and induced bone formation in the diabetic mice. Dkk1 was also increased in bones from diabetic mice in our study. However, the PTHrP peptides did not reverse this increased. The reason for the inability of the PTHrP peptides to decrease the upregulated expression of Dkk1 in T1D mice is not known at this time. However, earlier studies showed that similar PTHrP peptides decreased Dkk1 expression, which is elevated in ovariectomized mice [43]. In this previous study, the peptides were administered at higher doses than in the current study, for 4 and 8 weeks, and throughout the study until samples were collected. In our study, the peptides were given only for 3 days, and samples were collected 12 days after the last peptide injection. Therefore, it is possible that these differences in the therapeutic regimens combined with the different underlying pathology (ovariectomy versus diabetes) explain the differential effect of the peptides on Dkk1 expression.

The rationale for testing the effectiveness of PTHrP peptides in diabetic models is based on the pharmacologic ability of the peptides to stimulate bone formation [44], which is decreased with T1D [32]. Earlier studies showed that N-terminal PTHrP analogue (1-36) and the native C-terminal fragment of PTHrP, PTHrP(107-139), different analogs from the ones used here, elicited osteogenic effects in CD1 mouse

STZ-diabetic model, albeit at higher doses and after prolonged administration compared to the current experiment [4]. Our present study represents the first attempt to use an experimental maneuver combining short PTHrP treatment with mechanical loading as a strategy to promote bone formation in diabetes. Regarding the receptors activated by each PTHrP peptide used in our study, the anabolic actions of all peptides comprising N-terminal domains of PTHrP tested so far are mediated through the PTH1R in osteoblast lineage cells, including osteocytes, and mainly involve cAMP as well as non-classical PTH1R-dependent signaling pathways such as MAPK activation [5,14]. In contrast, antagonizing the PTH1R does not alter the action of peptides comprising the C-terminal domains of PTHrP, which appear to be related to VEGFR2 transactivation in osteoblasts [5,45,46]. Consistent with this earlier evidence, we now show that silencing the PTH1R in osteocytic MLO-Y4 cells does not eliminate the antiapoptotic effect of PTHrP (107-111); and that a VEGFR2 activation inhibitor blocked the effect of PTHrP (107-111). These findings demonstrate that the protective effect of the PTHrP peptides is mediated by different mechanisms of action.

An earlier study showed additive, although moderate, efficacy of daily administration of PTH(1-34) together with mechanical loading in promoting periprosthetic cancellous bone accrual in rabbit femoral metaphysis [47]. The fact that mechanical or pharmacological stimuli independently decreased or stimulated osteoclastogenesis, respectively, might explain the mild effect on bone compared to the current study in which ulna loading and the PTHrP-derived peptides were shown to additively increase bone. Consistent with the current data, the peptides studied exhibited bone anabolic activity in mouse and rat cortical bone [44,48,49].

We recently reported that N-terminal PTHrP is similarly effective as mechanical loading to protect MLO-Y4 osteocytic cells from apoptosis [14]. Deleterious effects of

high glucose on various responses of this osteocytic cell line to fluid flow stimulation were also recently reported [8]. Our *in vitro* data show that PTHrP(1-37) and (107-111) were similarly effective to increase MLO-Y4 cell viability even in the presence of high glucose. Moreover, the impaired response to fluid flow-mechanical stimulus in the latter setting was also prevented by the peptides. Further, both the PTHrP peptides and fluid flow activated ERKs and induced β-catenin nuclear translocation. These findings are consistent with our previous evidence that N- and C-terminal domains of PTHrP enable β-catenin stabilization, which is hampered by high glucose, in osteoblastic cell cultures [42].

In summary, our findings collectively demonstrate that bone fragility induced by diabetes is due to a combination of increased bone resorption, decreased bone formation and decreased viability of osteocytes. Further, short treatment with the PTHrP-derived peptides ameliorates these effects and acts additively with mechanical stimulation to prevent bone fragility induced by diabetes **(Figure 9)**. This evidence highlights the potential of approaches that control bone remodeling and maintain viability and function of osteocytes in the treatment of diabetes-induced skeletal deterioration.

Acknowledgements

The authors thank Dr. Xiaolin Tu and Dr. Alexander G. Robling for providing training on ulnae loading, and Hannah M. Davis for technical support.

Author contributions: A.R.G., P.E. and T.B. designed research; M.M., K.W.C., A.Y.S., G.G., D.M.B. and M.R.A. performed research; M.M., L.I.P., A.R.G., P.E., and T.B. analyzed and interpreted data; M.M., L.I.P., A.R.G., P.E., and T.B. wrote the manuscript. P.E. and T.B. takes responsibility for the integrity of the data analysis. This research was supported by the National Institutes of Health (R01-AR059357 to T.B.); the Veterans Administration (1 I01 BX002104-01 to T.B.); the Spanish Instituto de Salud Carlos III (PI11/00449 and RD12/0043/0008); and Universidad San Pablo CEU (emerging group). M.M. received short-term fellowships from The European Molecular and Biology Organization (EMBO), Conchita Rábago Foundation, and Boehringer Ingelheim; and was also supported by Spanish Ministerio de Economía y Competitividad (FI12/00458).

References

1. Vestergaard P. Discrepancies in bone mineral density and fracture risk in patients with type 1 and type 2 diabetes--a meta-analysis. Osteoporos Int 2007;18:427-444.

2. Hofbauer LC, Brueck CC, Singh SK, Dobnig H. Osteoporosis in patients with diabetes mellitus. J Bone Miner Res 2007;22:1317-1328.

3. Jiao H, Xiao E, Graves DT. Diabetes and Its Effect on Bone and Fracture Healing. Curr Osteoporos Rep 2015;13:327-335.

4. Lozano D, de Castro LF, Dapia S et al. Role of Parathyroid Hormone-Related Protein in the Decreased Osteoblast Function in Diabetes-Related Osteopenia. Endocrinology 2009;150:2027-2035.

5. Esbrit P, Alcaraz MJ. Current perspectives on parathyroid hormone (PTH) and PTH-related protein (PTHrP) as bone anabolic therapies. Biochem Pharmacol 2013;85:1417-1423.

6. Bonewald LF. The Amazing Osteocyte. J Bone Miner Res 2011;26:229-238.

7. Bellido T. Osteocyte-Driven Bone Remodeling. Calcif Tissue Int 2013;94:25-34.

8. Parajuli A, Liu C, Li W et al. Bone's responses to mechanical loading are impaired in type 1 diabetes. Bone 2015;81:152-160.

9. Lai X, Price C, Modla S et al. The dependences of osteocyte network on bone compartment, age, and disease. Bone Res 2015;3.

10. Portal-Nunez S, Lozano D, de Castro LF et al. Alterations of the Wnt/beta-catenin pathway and its target genes for the N- and C-terminal domains of parathyroid hormone-related protein in bone from diabetic mice. FEBS Lett 2010;584:3095-3100.

11. O'Brien CA, Plotkin LI, Galli C et al. Control of bone mass and remodeling by PTH receptor signaling in osteocytes. PLoS ONE 2008;3:e2942.

12. Saini V, Marengi DA, Barry KJ et al. Parathyroid hormone (PTH)/PTH-related peptide type 1 receptor (PPR) signaling in osteocytes regulates anabolic and catabolic skeletal responses to PTH. J Biol Chem 2013;288:20122-20134.

13. Tu X, Pellegrini G, Galli C et al. PTH receptor 1 expression in osteocytes is indispensable for the anabolic effect of mechanical loading in mice. J Bone Miner Res 2011;26:S24.

14. Maycas M, Ardura JA, de Castro LF et al. Role of the parathyroid hormone type 1 receptor (PTH1R) as a mechanosensor in osteocyte survival. J Bone Miner Res 2015;30:1231-1244.

15. Sawakami K, Robling AG, Ai M et al. The WNT co-receptor LRP5 is essential for skeletal mechanotransduction, but not for the anabolic bone response to parathyroid hormone treatment. J Biol Chem 2006;281:23698-23711.

16. Tu X, Rhee Y, Condon KW et al. Sost downregulation and local Wnt signaling are required for the osteogenic response to mechanical loading. Bone 2012;50:209-217.

17. Robling AG, Turner CH. Mechanotransduction in bone: genetic effects on mechanosensitivity in mice. Bone 2002;31:562-569.

18. Tu X, Delgado-Calle J, Condon KW et al. Osteocytes mediate the anabolic actions of canonical Wnt/β-catenin signaling in bone. Proc Natl Acad Sci U S A 2015;112:E478-E486.

19. Rhee Y, Allen MR, Condon K et al. PTH receptor signaling in osteocytes governs periosteal bone formation and intra-cortical remodeling. J Bone Miner Res 2011;26:1035-1046.

20. Pacheco-Costa R, Davis HM, Sorenson C et al. Defective cancellous bone structure and abnormal response to PTH in cortical bone of mice lacking Cx43 cytoplasmic C-terminus domain. Bone 2015;81:632-643.

21. Dempster DW, Compston JE, Drezner MK et al. Standardized nomenclature, symbols, and units for bone histomorphometry: A 2012 update of the report of the ASBMR Histomorphometry Nomenclature Committee. J Bone Miner Res 2013;28:2-17.

22. Delgado-Calle J, Anderson J, Cregor MD et al. Bidirectional Notch signaling and osteocyte-derived factors in the bone marrow microenvironment promote tumor cell proliferation and bone destruction in multiple myeloma. Cancer Res 2016;76:1089-1100.

23. Kato Y, Windle JJ, Koop BA, Mundy GR, Bonewald LF. Establishment of an osteocyte-like cell line, MLO-Y4. J Bone Miner Res 1997;12:2014-2023.

24. Plotkin LI, Weinstein RS, Parfitt AM et al. Prevention of osteocyte and osteoblast apoptosis by bisphosphonates and calcitonin. J Clin Invest 1999;104:1363-1374.

25. Gortazar AR, Martin-Millan M, Bravo B, Plotkin LI, Bellido T. Crosstalk between caveolin-1/ERKs and ß-catenin survival pathways in osteocyte mechanotransduction. J Biol Chem 2013;288:8168-8175.

26. Sato AY, Cregor M, Delgado-Calle J et al. Protection from Glucocorticoid-Induced Osteoporosis by Anti-Catabolic Signaling in the Absence of Sost/Sclerostin. J Bone Miner Res 2016;doi: 10.1002/jbmr.2869.

27. Robling AG, Niziolek PJ, Baldridge LA et al. Mechanical stimulation of bone in vivo reduces osteocyte expression of Sost/sclerostin. J Biol Chem 2008;283:5866-5875.

28. Bellido T, Ali AA, Plotkin LI et al. Proteasomal degradation of Runx2 shortens parathyroid hormone-induced anti-apoptotic signaling in osteoblasts. A putative explanation for why intermittent administration is needed for bone anabolism. J Biol Chem 2003;278:50259-50272.

29. Amling M, Neff L, Tanaka S et al. Bcl-2 lies downstream of parathyroid hormone-related peptide in a signaling pathway that regulates chondrocyte maturation during skeletal development. J Cell Biol 1997;136:205-213.

30. Plotkin LI, Mathov I, Aguirre JI et al. Mechanical stimulation prevents osteocyte apoptosis: requirement of integrins, Src kinases and ERKs. Am J Physiol Cell Physiol 2005;289:C633-C643.

31. de Castro LF, Maycas M, Bravo B, Esbrit P, Gortazar A. VEGF Receptor 2 (VEGFR2) Activation Is Essential for Osteocyte Survival Induced by Mechanotransduction. J Cell Physiol 2015;230:278-285.

32. Motyl KJ, McCauley LK, McCabe LR. Amelioration of type I diabetes-induced osteoporosis by parathyroid hormone is associated with improved osteoblast survival. J Cell Physiol 2012;227:1326-1334.

33. Motyl KJ, Botolin S, Irwin R et al. Bone inflammation and altered gene expression with type I diabetes early onset. J Cell Physiol 2009;218:575-583.

34. Botolin S, McCabe LR. Bone loss and increased bone adiposity in spontaneous and pharmacologically induced diabetic mice. Endocrinology 2007;148:198-205.

35. Hamada Y, Kitazawa S, Kitazawa R et al. Histomorphometric analysis of diabetic osteopenia in streptozotocin-induced diabetic mice: a possible role of oxidative stress. Bone 2007;40:1408-1414.

36. Hie M, Iitsuka N, Otsuka T, Tsukamoto I. Insulin-dependent diabetes mellitus decreases osteoblastogenesis associated with the inhibition of Wnt signaling through increased expression of Sost and Dkk1 and inhibition of Akt activation. Int J Mol Med 2011;28:455-462.

37. Verhaeghe J, Thomsen JS, van BR et al. Effects of exercise and disuse on bone remodeling, bone mass, and biomechanical competence in spontaneously diabetic female rats. Bone 2000;27:249-256.

38. Botolin S, Faugere MC, Malluche H et al. Increased bone adiposity and peroxisomal proliferator-activated receptor-gamma2 expression in type I diabetic mice. Endocrinology 2005;146:3622-3631.

39. Wittrant Y, Gorin Y, Woodruff K et al. High d(+)glucose concentration inhibits RANKL-induced osteoclastogenesis. Bone 2008;42:1122-1130.

40. Motyl K, McCabe LR. Streptozotocin, type I diabetes severity and bone. Biol Proced Online 2009;11:296-315.

41. Portal-Nunez S, Ardura JA, Lozano D et al. Adverse Effects of Diabetes Mellitus on the Skeleton of Aging Mice. J Gerontol A Biol Sci Med Sci 2016;71:290-299.

42. Lopez-Herradon A, Portal-Nunez S, Garcia-Martin A et al. Inhibition of the canonical Wnt pathway by high glucose can be reversed by parathyroid hormone-related protein in osteoblastic cells. J Cell Biochem 2013;114:1908-1916.

43. de Castro LF, Lozano D, Portal-Nunez S et al. Comparison of the Skeletal effects induced by daily administration of PTHrP (1-36) and PTHrP (107-139) to ovariectomized mice. J Cell Physiol 2011.

44. Esbrit P, Herrera S, Portal-Nunez S, Nogues X, Diez-Perez A. Parathyroid Hormone-Related Protein Analogs as Osteoporosis Therapies. Calcif Tissue Int 2016;98:359-369.

45. Valin A, Guillen C, Esbrit P. C-terminal parathyroid hormone-related protein (PTHrP) (107-139) stimulates intracellular Ca(2+) through a receptor different from the type 1 PTH/PTHrP receptor in osteoblastic osteosarcoma UMR 106 cells. Endocrinology 2001;142:2752-2759.

46. Lozano D, Fernandez-de-Castro L, Portal-Nunez S et al. The C-terminal fragment of parathyroid hormone-related peptide promotes bone formation in diabetic mice with low-turnover osteopaenia. Br J Pharmacol 2011;162:1424-1438.

47. Grosso MJ, Courtland HW, Yang X et al. Intermittent PTH administration and mechanical loading are anabolic for periprosthetic cancellous bone. J Orthop Res 2015;33:163-173.

48. Rouffet J, Coxam V, Gaumet N, Barlet JP. Preserved bone mass in ovariectomized rats treated with parathyroid-hormone-related peptide (1-34) and (107-111) fragments. Reprod Nutr Dev 1994;34:473-481.

49. Rodriguez-de la Rosa L, Lopez-Herradon A, Portal-Nunez S et al. Treatment with N- and C-terminal peptides of parathyroid hormone-related protein partly compensate the skeletal abnormalities in IGF-I deficient mice. PLoS ONE 2014;9:e87536.

Figure legends

Figure 1. T1D mice exhibit decreased BMD and weakened bone microarchitecture that is corrected by PTHrP-derived peptides. (A) Experimental scheme showing the animal model protocol, indicating the point in which the experiment started (t0), when mechanical loading/peptide administration started (t1) and the time of sacrifice (t2). (B) Glucose levels and body weight measured in blood from mice at t2. (C) Total, spine and femur BMD at t1. (D) Percent change in spine and femur BMD from t0 to t1. (E) Percent change in spine and femur BMD from t1 to t2. n= 28-30 per group. (F and G) Analysis and representative images of bone microarchitecture by μCT in cortical (femoral mid-diaphysis) and cancellous (distal femur). n= 7-10 per group. Scale bars indicate 500 μm. Bars represent mean ± SD,*$p<0.05$ versus control mice, $^{\#}p<0.05$ versus T1D, by one-way ANOVA.

Figure 2. T1D mice exhibit decreased osteoblasts and bone formation and increased osteoclasts and these effects are reversed by PTHrP-derived peptides. (A) Osteoblasts, osteoclasts and osteocytes were identified in mice bone sections from lumbar vertebrae stained by von Kossa/McNeal. Number of osteoblasts per bone surface (NOb/BS), surface covered by osteoblasts (ObS/BS), osteoclast number per bone surface (NOc/BS), surface covered by osteoclasts (OcS/BS), eroded surface per bone surface (ES/BS) and osteocyte number per bone volume (NOt/BV), were reported. Bars represent mean ± SD, n= 7-10 per group. Dynamic bone histomorphometric analysis was performed in (B) the cancellous surface of lumbar vertebrae and (C) endocortical surface of the ulna mid-diaphysis. Mineralizing surface (MS/BS), mineral apposition rate (MAR) and bone formation rate (BFR) were measured in unstained sections. (B) n= 6-10 per group, (C) n= 19-24 per group. Bars represent mean ± SD, *$p<0.05$ versus control mice, $^{\#}p<0.05$ versus vehicle-treated T1D mice, by one-way ANOVA.

Representative images of von Kossa/McNeal stained (A) and fluorescent images (B) of bone sections are shown. White arrows point at osteoblasts (ob), osteoclasts (oc) or osteoid (os). Scale bars indicate 500 μm.

Figure 3. T1D mice exhibited defective mechanical and material properties, which are restored by treatment with PTHrP-derived peptides. (A) Mechanical and (B) material properties were measured in the femoral mid-diaphysis by 3-point bending testing. n= 7-10 per group. Bars represent mean ± SD, * $p<0.05$ versus control mice, # $p<0.05$ versus vehicle-treated T1D mice, by one-way ANOVA.

Figure 4. PTHrP-derived peptides counteract the changes in bone resorption and formation markers and in bone gene expression induced by T1D. (A) C-telopeptide fragments of type I collagen (CTX) and osteocalcin (OCN) measured at the end of the study in serum and plasma, respectively. (B-D) Expression of the the osteoblast marker osterix, and the Wnt/β-catenin antagonists, dkk1 and Sost, cytokines OPG and RANKL and the RANKL/OPG ratio, the osteoclast marker TRAP, Cx43, PTHrP and PTHR1 in tibia. n= 7-10 per group. Bars represent mean ± SD, * $p<0.05$ versus control mice, # $p<0.05$ versus vehicle-treated T1D mice, by one-way ANOVA.

Figure 5. T1D mice exhibit increased marrow adiposity, which is reduced by the PTHrP peptides. (A) Areas covered by adipocytes were measured in ulnae mid-diaphysis and corrected by marrow area. n= 5-6 mice per group. Bars represent mean ± SD, * $p<0.05$ versus non diabetic control mice and # $p<0.05$ versus T1D mice, by one-way ANOVA. **(B)** Representative images are shown. Scale bar indicates 25 μm.

Figure 6. T1D mice exhibit decreased sensitivity to loading, which is restored by PTHrP-derived peptides alone and additively with mechanical stimulation. Bone histomorphometric measurements were performed on non-loaded and loaded ulnae at

(**A**) low (1,995 με), (**B**) medium (2,250 με), and (**C**) high (2,500 με) magnitudes of strain. n= 5-8 per group. Bars represent mean ± SD, * $p<0.05$ versus the corresponding non-loaded mice by paired t-test. # $p<0.05$ versus loaded saline mice, [a] $p<0.05$ versus corresponding (loaded or non-loaded) vehicle-treated T1D mice, by two-way ANOVA. Representative fluorescent images corresponding to the highest intensity are shown. Scale bar indicates 500 μm.

Figure 7. Loading decreases sclerostin and both loading and the PTHrP peptides reverse T1D-induced osteocyte apoptosis *in vivo*. Osteocytes from non-loaded and loaded ulnae cross sections at low, medium, and high magnitude of strain were stained and scored for (**A**) and (**B**) sclerostin and (**C**) TUNEL, to determine apoptosis. n= 5-8 per group. Bars represent mean ± SD, *$p<0.05$ versus the corresponding non-loaded mice by paired t-test. #$p<0.05$ versus loaded saline mice, [a]$p<0.05$ versus corresponding (either loaded or non-loaded) T1D vehicle-treated mice, by two-way ANOVA.

Figure 8. Mechanical stimulation and PTHrP peptides elicit pro-survival signals *in vitro* (**A**) MLO-Y4 osteocytic cells expressing nGFP exposed to normal glucose or high glucose (25 mM) and with or without PTHrP-derived peptides were subjected to fluid flow or static control conditions and apoptosis was quantified by nuclear morphology. PTHrP did not change the number of living cells. (**B**) MLO-Y4 cells silenced for PTH1R or treated with scramble siRNA were treated with the specific VEGFR2 inhibitor SU5416 for 30 min and subsequently with PTHrP (107-111) for additional 30 min. Cell viability was measured after etoposide addition, as described in Materials and Methods. Bars represent mean ± SD of 3 experiments carried out in duplicate, *$p<0.05$ versus corresponding vehicle-treated cells, by one-way ANOVA followed by Tukey test. (**C** and **D**) Bcl-2, β-catenin, and ERK nuclear protein levels were quantified by Western blotting. The dividing lines in the β-catenin and lamin B1 western blot indicate

different parts of the same gel. Bars represent mean ± SD of 2-3 experiments carried out in duplicate (Bcl-2) or triplicate (β-catenin and ERKs), *$p<0.05$ versus normal glucose, static control; $^{\#}p<0.05$ versus high glucose, static control; $^{a}p<0.05$ versus high glucose, fluid flow, by Kruskal-Wallis test followed by Mann-Whitney test.

Figure 9. Working model. PTHrP(1-37) or PTHrP(107-111) reversed the skeletal deterioration in T1D, partially restoring the loss of bone mass and strength, and reversing the decreased bone formation and increased Sost expression and resorption. Furthermore, the PTHrP peptides worked additively with mechanical loading to enhance periosteal bone formation and reduce osteocytic apoptosis in the appendicular skeleton of diabetic mice.

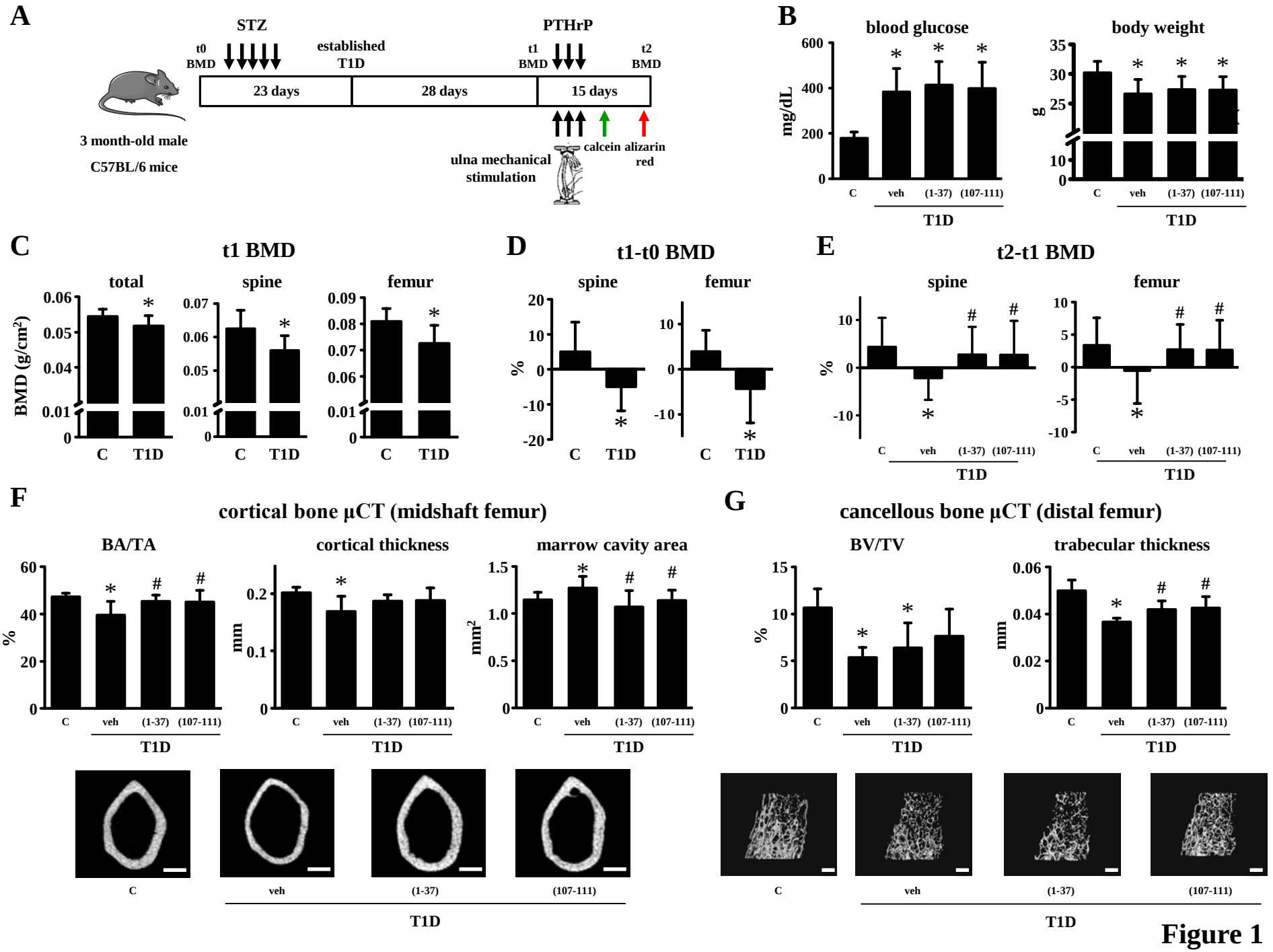
A
STZ
PTHrP
t0 BMD
established T1D
t1 BMD
t2 BMD
23 days
28 days
15 days
3 month-old male C57BL/6 mice
ulna mechanical stimulation
calcein
alizarin red
B
blood glucose
mg/dl
body weight
g
C
veh
(1-37)
(107-111)
T1D
C
t1 BMD
total
spine
femur
BMD (g/cm²)
D
t1-t0 BMD
spine
femur
%
E
t2-t1 BMD
spine
femur
%
F
cortical bone µCT (midshaft femur)
BA/TA
%
cortical thickness
mm
marrow cavity area
mm²
G
cancellous bone µCT (distal femur)
BV/TV
%
trabecular thickness
mm

Figure 1

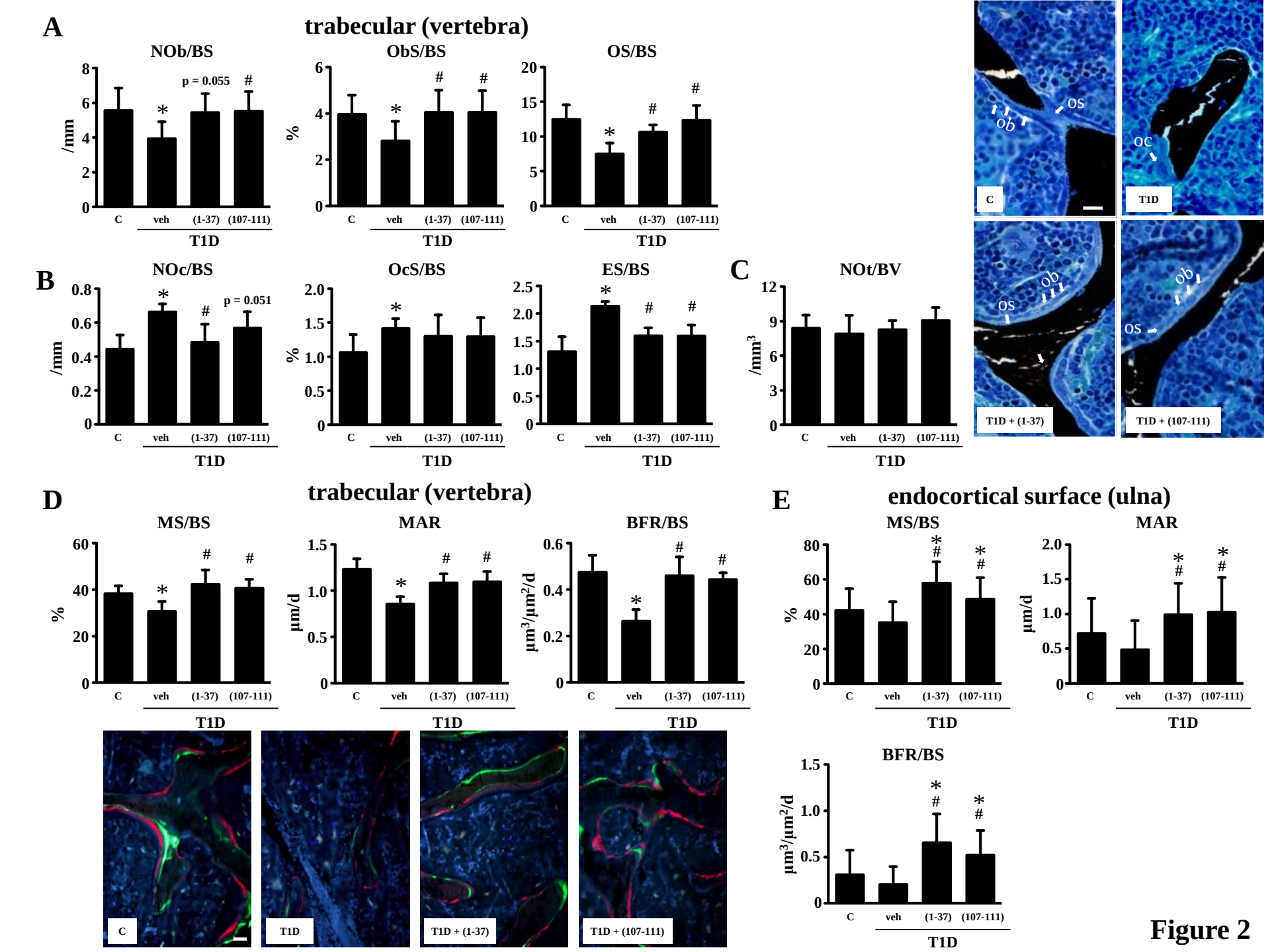
A
trabecular (vertebra)
NOb/BS
/mm
p = 0.055
ObS/BS
%
OS/BS
C
veh
(1-37)
(107-111)
T1D
B
NOc/BS
p = 0.051
OcS/BS
ES/BS
C
NOt/BV
/mm3
os
ob
oc
T1D + (1-37)
T1D + (107-111)
D
trabecular (vertebra)
MS/BS
MAR
BFR/BS
µm/d
µm3/µm2/d
E
endocortical surface (ulna)

Figure 2

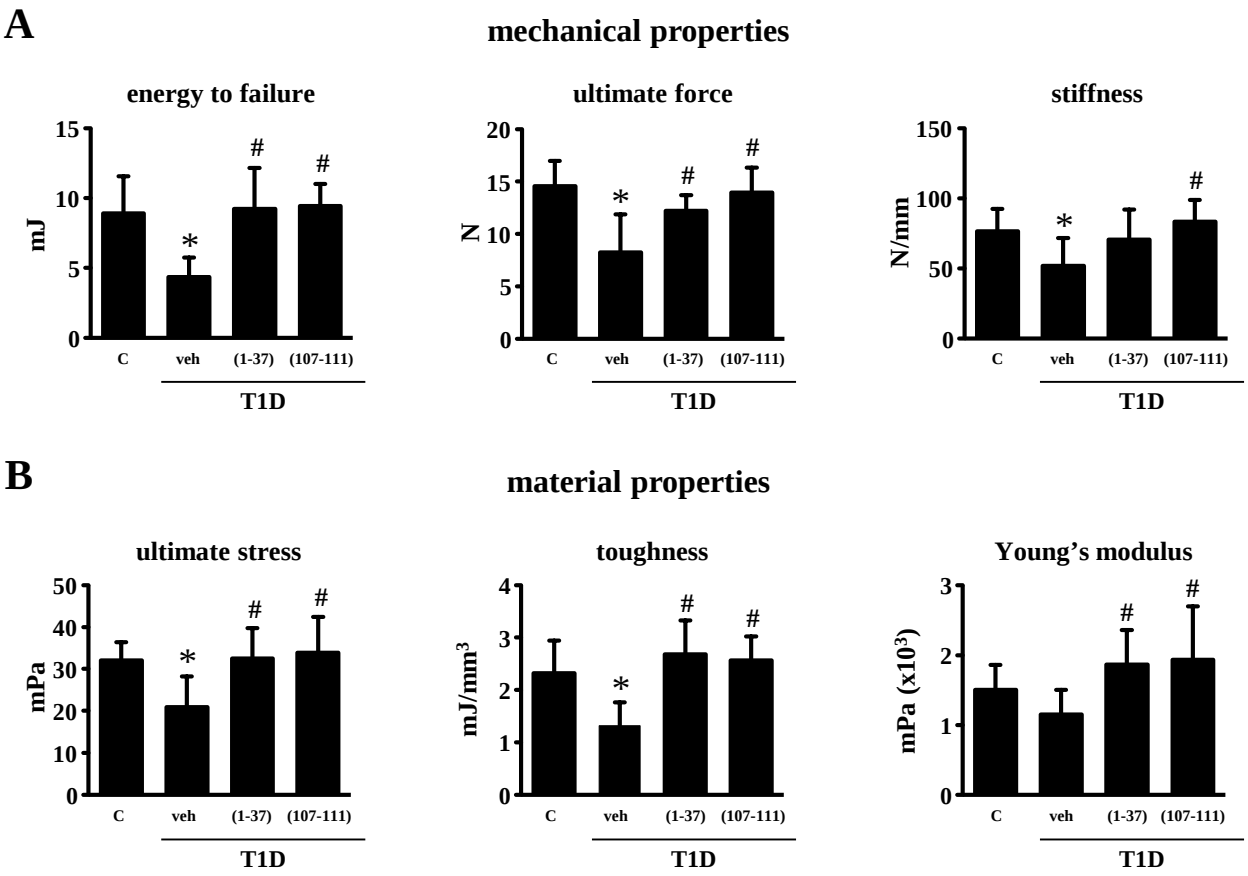
A
mechanical properties
energy to failure
mJ
15
10
5
0
*
#
#
C
veh
(1-37)
(107-111)
T1D
ultimate force
N
20
15
10
5
0
*
#
#
C
veh
(1-37)
(107-111)
T1D
stiffness
N/mm
150
100
50
0
*
#
C
veh
(1-37)
(107-111)
T1D
B
material properties
ultimate stress
mPa
50
40
30
20
10
0
*
#
#
C
veh
(1-37)
(107-111)
T1D
toughness
mJ/mm3
4
3
2
1
0
*
#
#
C
veh
(1-37)
(107-111)
T1D
Young's modulus
mPa (x10^3)
3
2
1
0
#
#
C
veh
(1-37)
(107-111)
T1D

Figure 3

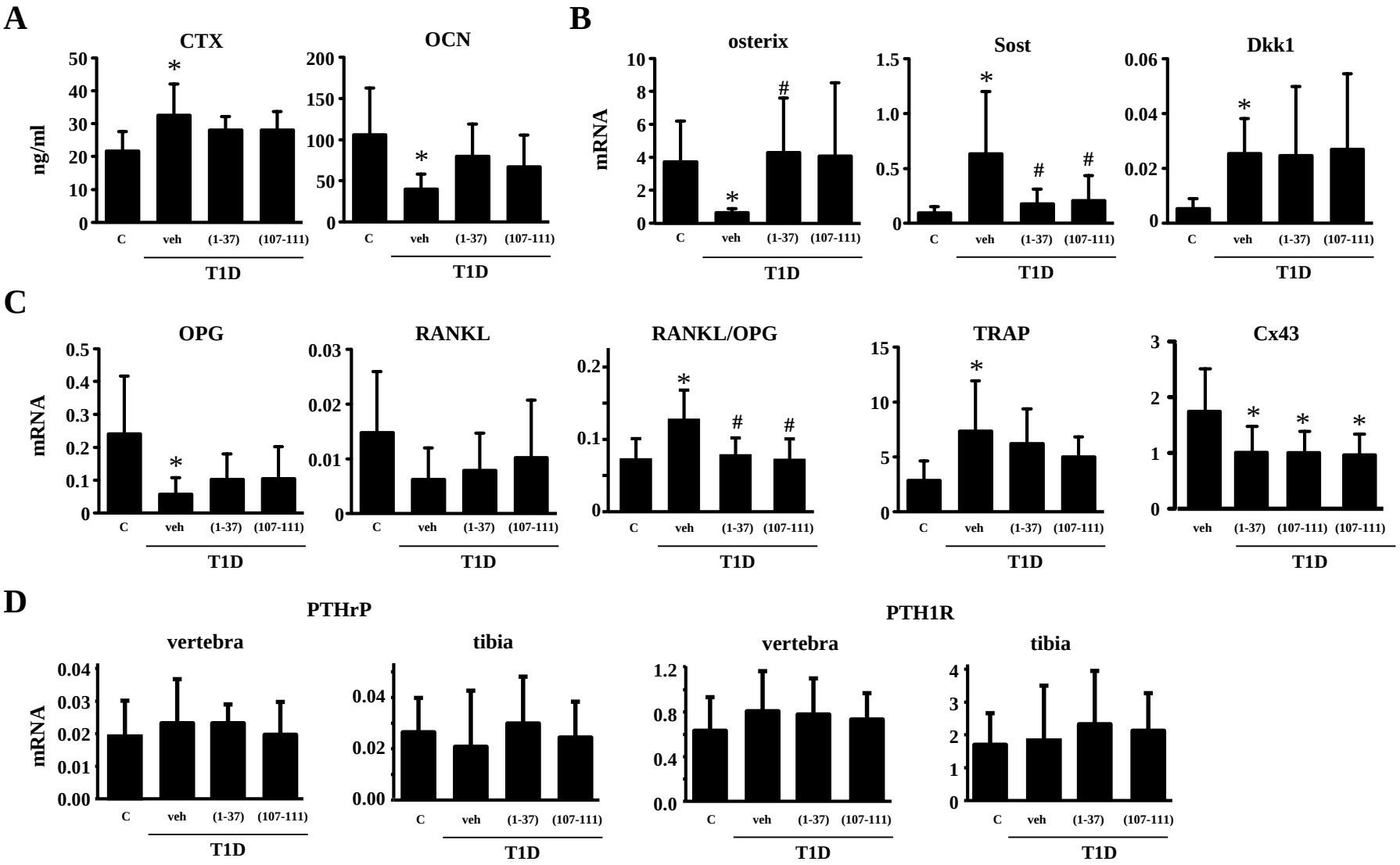
A
CTX
ng/ml
OCN
B
osterix
Sost
Dkk1
mRNA
C
OPG
RANKL
RANKL/OPG
TRAP
Cx43
D
PTHrP
PTH1R
vertebra
tibia
C
veh
(1-37)
(107-111)
T1D

Figure 4

A

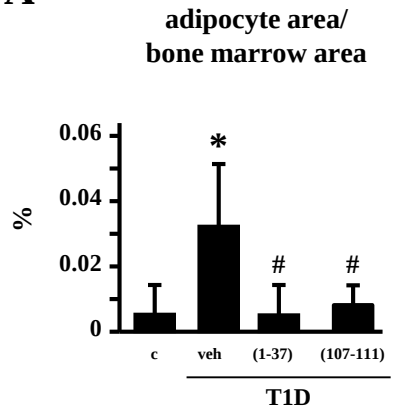
adipocyte area/
bone marrow area
0.06
0.04
0.02
0
%
*
#
#
c
veh
(1-37)
(107-111)
T1D

B

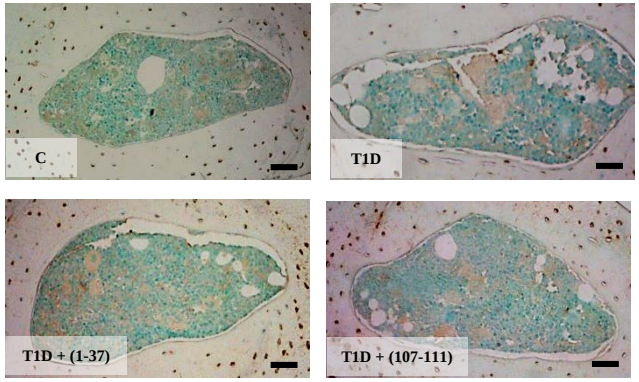
C
T1D
T1D + (1-37)
T1D + (107-111)

Figure 5

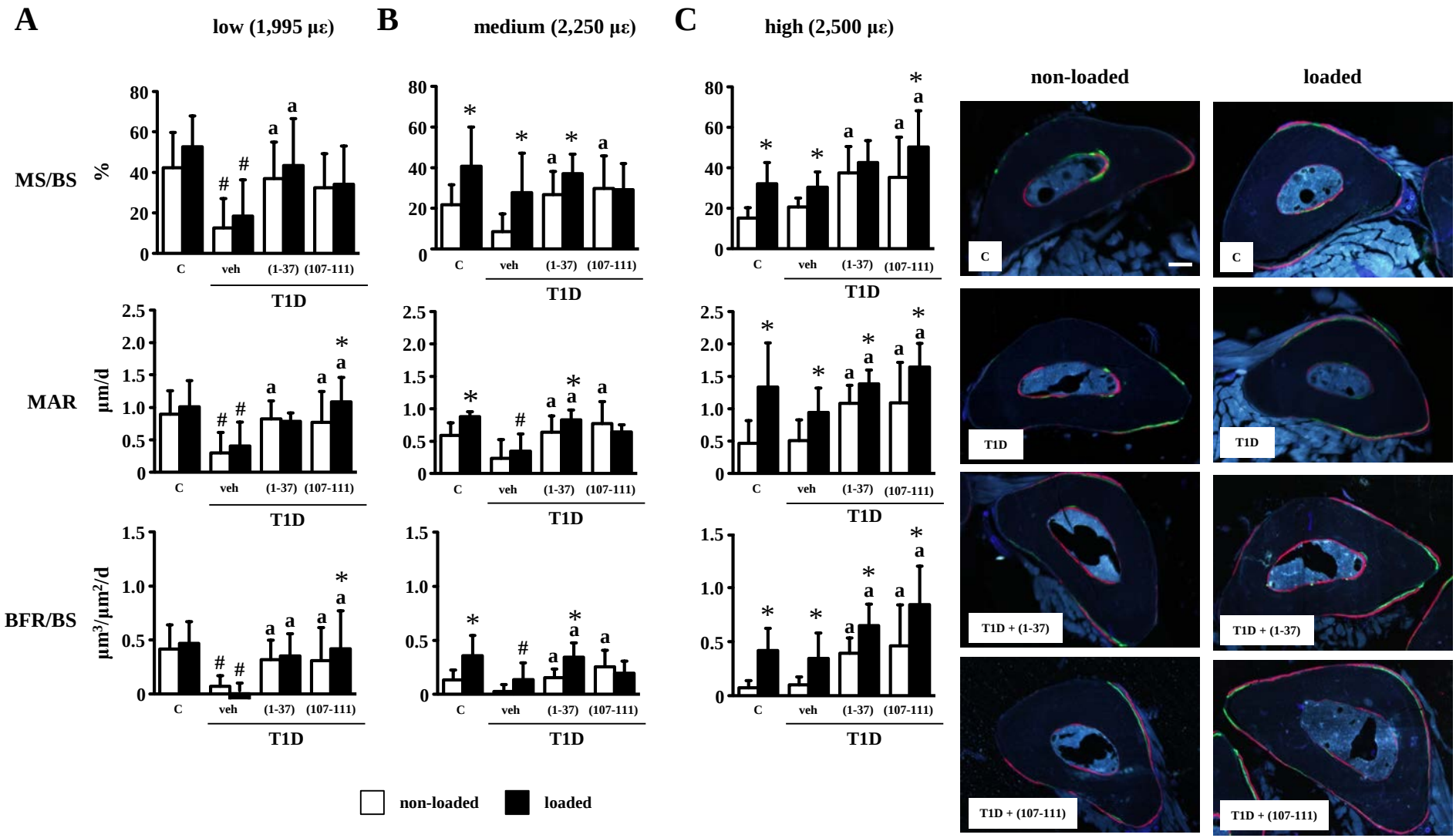
A
low (1,995 με)
B
medium (2,250 με)
C
high (2,500 με)
MS/BS
%
MAR
μm/d
BFR/BS
μm³/μm²/d
C
veh
(1-37)
(107-111)
T1D
non-loaded
loaded
T1D + (1-37)
T1D + (107-111)

Figure 6

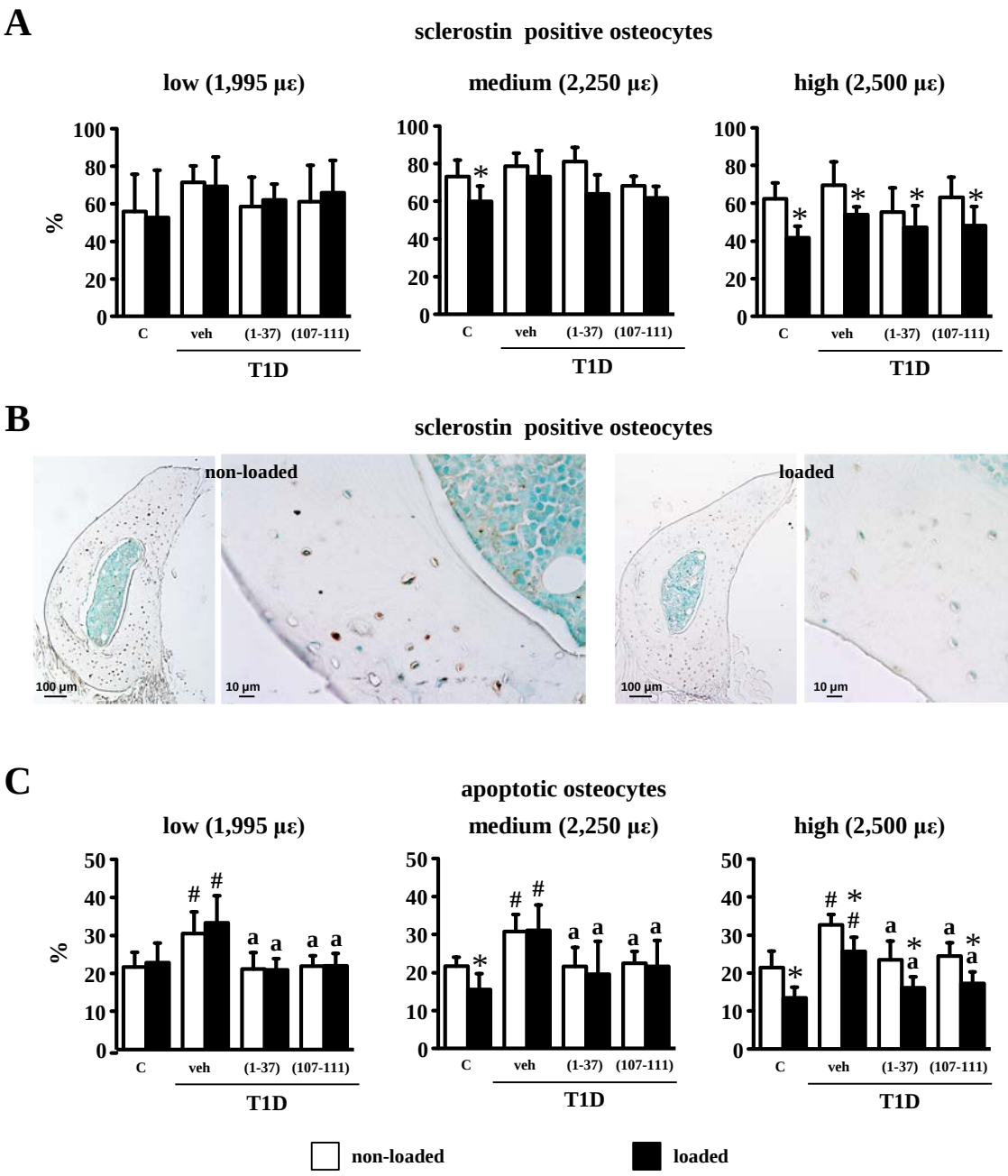
A
sclerostin positive osteocytes
low (1,995 με)
medium (2,250 με)
high (2,500 με)
%
C
veh
(1-37)
(107-111)
T1D
B
sclerostin positive osteocytes
non-loaded
loaded
100 μm
10 μm
C
apoptotic osteocytes
low (1,995 με)
medium (2,250 με)
high (2,500 με)
non-loaded
loaded

Figure 7

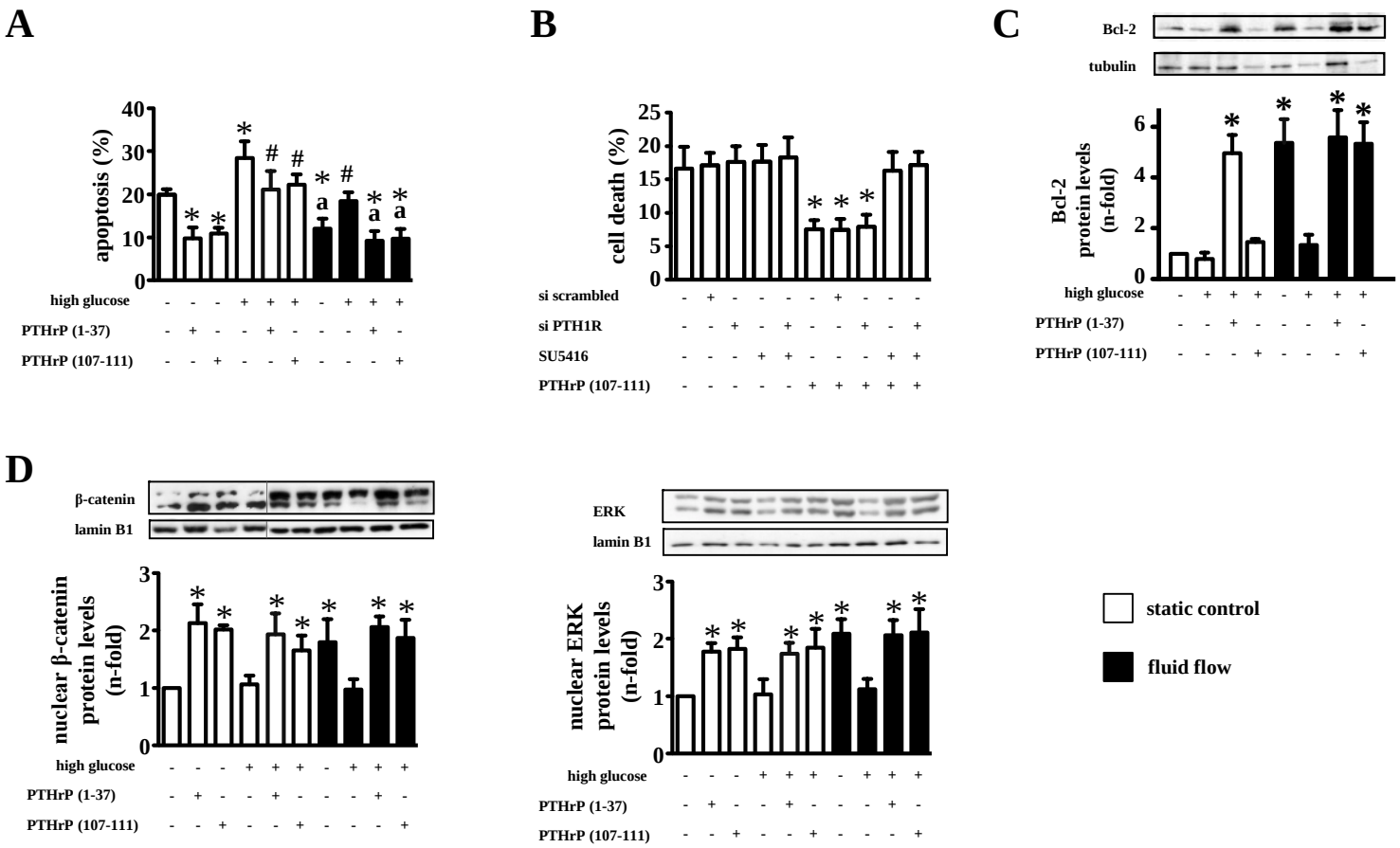
A
apoptosis (%)
high glucose
PTHrP (1-37)
PTHrP (107-111)
B
cell death (%)
si scrambled
si PTH1R
SU5416
PTHrP (107-111)
C
Bcl-2
tubulin
Bcl-2 protein levels (n-fold)
high glucose
PTHrP (1-37)
PTHrP (107-111)
D
β-catenin
lamin B1
nuclear β-catenin protein levels (n-fold)
high glucose
PTHrP (1-37)
PTHrP (107-111)
ERK
lamin B1
nuclear ERK protein levels (n-fold)
high glucose
PTHrP (1-37)
PTHrP (107-111)
static control
fluid flow

Figure 8

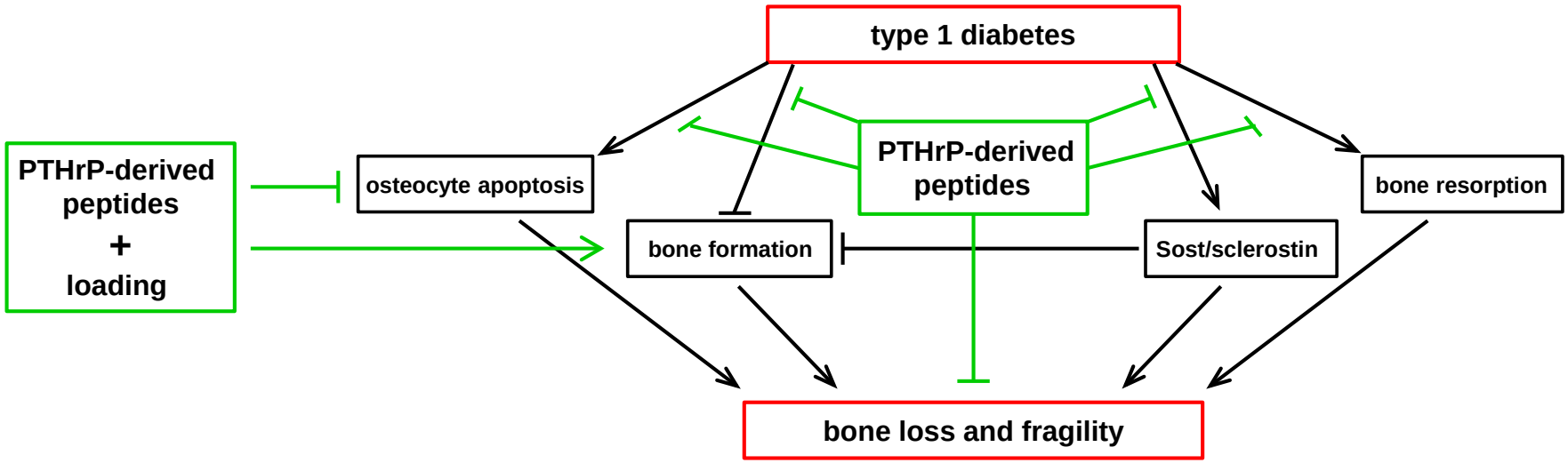
type 1 diabetes
PTHrP-derived peptides + loading
osteocyte apoptosis
PTHrP-derived peptides
bone resorption
bone formation
Sost/sclerostin
bone loss and fragility

Figure 9